Mating and Piercing Micromechanical Structures for Surface Bonding Applications

Hongtao Han*, Lee E. Weiss†, and Michael L. Reed*
Carnegie Mellon University
Pittsburgh, PA 15213-3890 USA

Abstract

We have developed two types of micromechanical structures, using silicon micromachining techniques, which act as mechanical adhesives. Arrays of structures are fabricated on standard silicon wafers, with an areal density of approximately 200,000 per cm^2, resulting in very strong bonds. Individual components are the order of 4-18 μm wide, and 4-15 μm high above the substrate. Mating structures, which interlock with themselves, and piercing structures, which interlock with biologic tissues, have been fabricated and tested. The mechanical behavior of this "micromechanical velcro" is in approximate agreement with the calculated strength.

Introduction

We have applied silicon micromachining technology to fabricate dense regular arrays of microstructures which act as surface adhesives. The principle of bonding is that of a button snap, or a zipper, but in a two-dimensional configuration. These arrays have applications in areas as diverse as integrated circuit bonding and vascular anastomosis.

The mating structures are shown in the micrograph of Figure 1. When identical wafers are aligned face-to-face, compressive loading causes the tabs to deform, spring back, and interlock. Minimum loads of approximately 12 kPa are necessary to bond the substrates together. Tensile strength of the bond is in excess of 240 kPa. We have verified that the bonding is due to interlocking by a variety of techniques, including direct examination in an electron microscope. We are currently applying this technology to mounting integrated circuit chips directly to an interconnecting substrate. The micromechanical fastening system has several advantages: high strength; simultaneous electrical, mechanical, and thermal contacting; high precision self-alignment; room temperature bonding.

A piercing structure is shown in Figure 2. Like the mating structures, this version is fabricated with a two mask process, and consists of SiO_2 caps on silicon pedestals. The very sharp point (radius of curvature is less than 0.1 μm) enables the structure to pierce biologic tissues; the reentrant supporting profile enables the structure to latch, preventing retraction. These microscopic barbs, fabricated on opposite sides of a silicon substrate, provide an ideal mechanism for joining tissues with minimal cellular damage.

*Department of Electrical and Computer Engineering
†Robotics Institute

Figure 1: Mating micromechanical structures. The caps are 1.0 μm SiO_2 on silicon pedestals.

In the following sections, we will describe the fabrication process, mechanical testing, and the theoretical limits of the mating microstructures; we will then describe our experimental efforts in tissue bonding with the piercing arrays.

Fabrication Process

Figure 3 illustrates the process sequence. A 1200 Å SiO_2 layer is grown at 1000 °C in dry oxygen on (100) silicon wafers. The oxide is patterned into an array of 10 μm square islands, with one edge aligned parallel to the (110) flat. After photoresist stripping, the wafer is immersed into an anisotropic etch bath consisting of aqueous KOH (33-45 %, 84 °C) and isopropyl alcohol. The etching results in a truncated pyramid or frustrum with exposed (212) planes, which are the fastest etching surfaces. [1] The (212) planes intercept the (100) base plane

CH2957-9/91/0000-0253$01.00 © 1991 IEEE

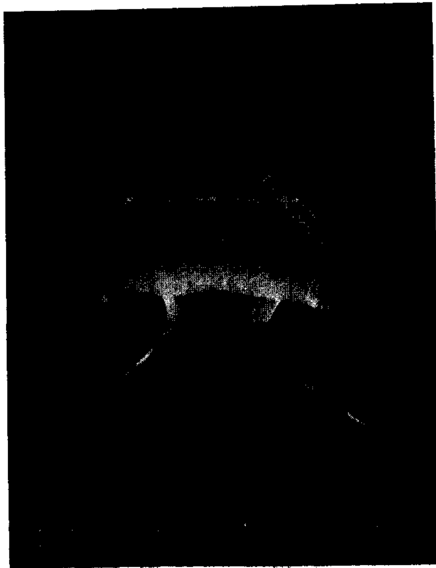

Figure 2: Piercing micromechanical structure for joining tissues.

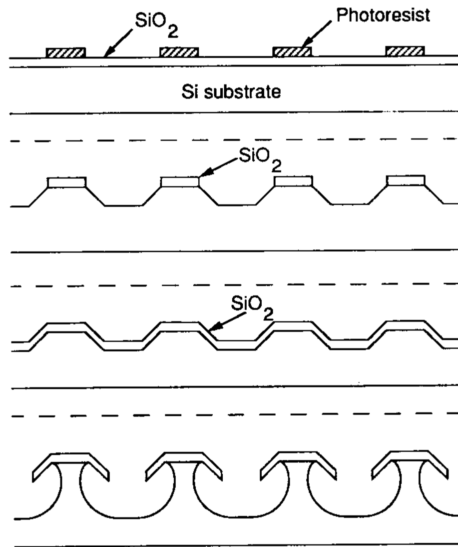

Figure 3: Fabrication process. Oxidized silicon substrates are patterned with photoresist, which act as a mask for an anisotropic silicon etch. After reoxidation and masking, an isotropic silicon etch defines the microstructures.

at an angle of 48°.

After stripping the masking oxide, and cleaning the samples with a conventional chemical sequence, a thick SiO_2 film, about 1.0-1.5 μm , is grown at 1000° C in wet oxygen. The oxide is patterned by a second mask consisting of an array of Greek crosses, each approximately 18 μm wide, aligned to the original array. The SiO_2 crosses act as a mask for a second etch in KOH which removes some of the underlying silicon. Finally, the microstructures are completed by etching the wafer in an isotropic planar etching bath (15:5:2 HNO_3:CH_3COOH:HF) for $\approx$ 1 minute. This step provides the vertical clearance for the interlocking mating structures, and the lateral undercut necessary to produce the four overhanging arms.

The process sequence for the piercing structures is similar. To achieve a pointed pyramid, the first etch is continued until the SiO_2 masking layer lifts off. The second level lithography reuses the first level mask, with a significant lateral overetch of the SiO_2 cap, to produce the structure shown in Figure 2.

The second masking step in both processes poses particular difficulties, especially for the pointed structures, since the surface is highly nonplanar after the first mask. We have successfully patterned the wafers by using a nominal 2.1 μm thick photoresist film, combined with a long exposure time (double the ordinary exposure energy). The resist thickness, as measured from electron micrographs, is highly nonuniform; it reaches about 3.0 μm in the field regions, and is severely thinned over the tops of the frustums. However, there is adequate thickness to prevent the buffered HF etchant from attacking the SiO_2 caps.

The isotropic silicon etch after the second mask step results in considerable lateral undercutting. To prevent this encroachment from weakening the silicon "posts" supporting the SiO_2 "caps", we use two techniques: 1) the inside corners of the Greek cross mask pattern are filleted to reduce the undercutting; and 2) the isotropic etch is preceeded by an anisotropic etch in KOH, as described above. This step reduces the undercutting by supplying most of the needed vertical clearance, without compromising the integrity of the silicon support.

Although the microstructures themselves are tiny, useful bonding strengths are realized when macroscopic scale arrays are utilized. Our present design uses a pitch of 22 μm , which results in areal density of over 200,000 per cm^2. Clearly, the array regularity will be compromised unless a superb mask set, with minimum runout error, is used to generate the patterns. The masks were fabricated at the National Nanofabrication Facility (at Cornell University) using an optical pattern generator and a reducing step and repeat camera; each mask contains over 5 million patterns across the 5 cm $\times$ 5 cm field.

Mechanical Testing

The bond strength of the mating structures was characterized by direct measurements of the tensile load needed to induce failure. Our investigations with these microstructures are at an early stage; thus, the results described here should be considered preliminary and on the conservative side.

Patterned samples, nominally 8 mm × 8 mm, were mounted on glass microscope slides using cyanoacrylate adhesive. The mating surfaces were placed together in rough azimuthal alignment, as observed with a low power microscope. Slight shaking of the samples was sufficient to precisely align the microstructures into a mating position. Interlocking was accomplished by applying pressure to the upper substrate; the loading force was monitored by placing the entire assembly on an electronic scale. Bonding was considered to have taken place once the weight of the lower sample and glass slide could be supported by the upper sample. The minimum load necessary for interlocking correspondings to a pressure of 12 kPa. (This compares to a value of 7×10^5 kPa which is needed to crush the silicon wafers.)

Bond strength was determined by applying a tensile load through a pulley and measuring the force necessary for separation. We find that separation of the samples is always accompanied by damaged areas on corresponding regions of the mating surfaces. An optical micrograph of a separated surface is shown in the Figure 4. Closeups of the microstructures in these areas reveal fracturing of the SiO_2 tabs near the interface with the silicon support post. We interpret this as evidence the samples are interlocking only over the damaged region. Furthermore, the fraction of damaged area is proportional to the initial loading. For example, a loading of 110 kPa results in an interlocked area of 13 %; increasing the insertion load to 330 kPa causes 21 % of the microstructures to latch. In addition to insufficient loading, partial interlocking could also be caused by particulate contamination which prevents uniform loading of the samples.

Taking the ratio of applied load to the sample area, we observe tensile strengths on the order of 10-250 kPa. However, if these values are corrected by the fraction of interlocked area, as estimated from the pattern of damage after separation, the tensile strength per unit of interlocked area is higher, about 400-1100 kPa. These values are in approximate agreement with the calculated strength, as described in the next section.

It is well known that silicon wafers placed in intimate contact will bond to each other, especially if moisture is present. [2, 3, 4, 5] To distinguish this phenomenon from the latching mechanism, we repeated our measurements with wafers without the arrays of microstructures. Depending on the surface treatment (native oxide, thermal oxide, HF-dipped) and the relative humidity (38%-100%), the tensile strength of the the bonded pairs varied from 12 to 20 kPa, well below the strength of the patterned samples. Similar results were obtained when the microstructure arrays were grossly misaligned. Figure 5 shows two interlocked samples, as viewed from above the edge of the upper sample. Close examination of this and other regions confirms that the bonding is indeed due to latching of the microstructure tabs.

Figure 4: Optical micrograph of sample surface after separation. The dark (damaged) areas are regions where the microstructure tabs have broken.

Calculation of Tensile Strength

An approximate calculation of the expected tensile strength is outlined in Figure 6. For simplicity, we consider a one dimensional cantilevered beam model, where the coupling between the four flanges of the Greek cross is neglected. Ignoring frictional forces, an applied external tensile force F_{ext} (per unit area) results in a force on each microstructure beam of

$$P_n = \frac{F_{ext} d^2}{4 \sin \alpha} \tag{1}$$

where P_n is the force acting normal to the beam, and $4/d^2$ is the areal density of cantilevered beams (4 beams on each structure, placed in a square array d cm apart). The distributions of shear force and bending moment along the beam are given by [6, 7, 8]:

$$\frac{dV(x)}{dx} = q(x) \tag{2}$$

$$\frac{dM(x)}{dx} = V(x) \tag{3}$$

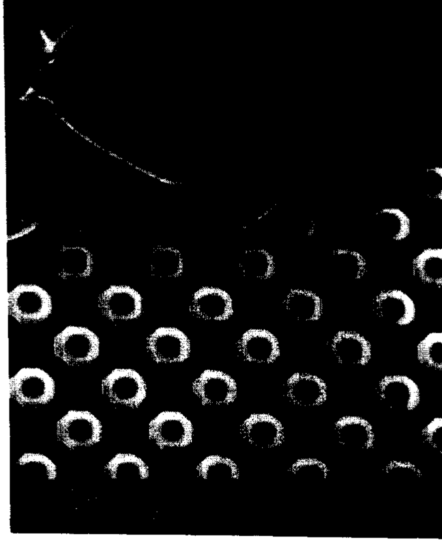

Figure 5: Electron micrograph of mated structures (top-down view along edge).

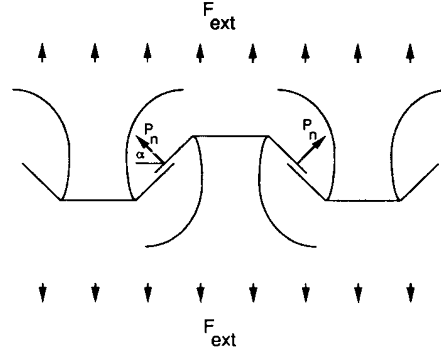

Figure 6: Nomenclature for force calculation. F_{ext} is the external applied force; P_n is the normal force on the microstructure tab; α is the angle between P_n and the substrate plane.

where $V(x)$, $M(x)$ and $q(x)$ are the shear force, bending moment and length density of the distributed force acting on the beam at position x. Omitting the gravitational force on the beam, the shear force and bending moment will take the simple form: $V(x) = -P_n$, $M(x) = P_n l - P_n x$. Therefore the fixed end of the cantilever beam suffers the maximum bending moment, which is equal to $P_n l$. The bending moment will result in deformation of the beam, which causes extension and compression on the convex side and the concave side respectively. The corresponding internal stress due to the bending is related to the bending moment by the flexure formula:

$$\sigma_x = \frac{M(x)y}{I_z} \tag{4}$$

where I_z represents the moment of inertia of the cross-sectional area about the centroidal axis, which is equal to $bh^3/12$ for a rectangular cross-section with width b and thickness h. Although this equation is derived for pure bending, it is still a good approximation with the presence of induced shearing stresses. [8] According to the flexure formula, the maximum stresses in the beam will occur at points furthest from the neutral axis, at $y = h/2$. Therefore, for the rectangular beam with height h, the maximum bending stress equals

$$\sigma_{max} = \frac{M(0)}{I_z}\frac{h}{2} = \frac{3F_{ext}d^2 l}{2bh^2 \sin\alpha} \tag{5}$$

and when this stress reaches the yield point stress of the flange material, σ_{yp}, the beam will break. At the yield point of the beam, the applied external force which describes the bonding strength is given by:

$$F_{ext} = \frac{2\sigma_{yp} bh^2 \sin\alpha}{3d^2 l} \tag{6}$$

If friction between the interlocked flanges is taken into account, the above equation is modified by a term representing the frictional force contribution:

$$F_{ext} = \frac{2\sigma_{yp} bh^2 \sin\alpha}{3d^2 l}(1 + \mu \cot\alpha) \tag{7}$$

where μ is the coefficient of static friction.

Substituting our design values in the above equation, ($b = 10$ μm, $h = 1$ μm, $l = 7.5$ μm, $\alpha = 42°$, $d = 22$ μm) and taking $\mu = 0.5$ and $\sigma_{yp} = 6.0 \times 10^5$ kPa [9], yields a tensile strength of $F_{ext} = 1.1 \times 10^3$ kPa. This value is at the upper end of the range of our present experimental measurements.

A more rigorous calculation would include other effects, such as the coupling between flanges, the weight of the flanges, and a short beam correction. Qualitatively, the coupling between flanges will change the stress and bending moment distribution as to increase the strength of the microstructures. This, plus the effect of static friction, yields a calculated strength which errs on the conservative side.

Stored Strain Energy

Two surfaces bonded together generally separate by crack propagation. The strength of the bond can be quantified by the magnitude of the energy associated with the

surface. There exists a way to relate the surface energy and the fracture length [10], but there is no satisfactory method of relating the surface energy to the tensile strength.

However, this limitation does not apply for the microstructure arrays, since the failure mode is not a fracture mechanism, but a more macroscopic yielding behavior. Therefore, the energy associated with the bond can be calculated by determining the work required to strain the array of cantilevers into yielding. This work represents the stored strain energy in the SiO_2 beams just before they break. This calculation is useful because it provides a way to compare the bond strength of the micromechanical fastening system with other surface bonding technologies.

From elementary beam theory [8], the strain energy stored in the deflected beam by bending can be expressed as:

$$U = \int_0^l \frac{[M(x)]^2}{2EI_z} dx \tag{8}$$

where U is strain energy stored in the single deflected cantilever beam, and E is Young's modulus. For $M(x) = P_n(l - x)$, we have:

$$U = \frac{P_n^2 l^3}{6EI_z} \tag{9}$$

U can also be expressed in the term of σ_{max} as

$$U = \frac{1}{9}(bhl)\frac{\sigma_{max}^2}{2E} \tag{10}$$

Accordingly, the "surface energy", which represents the strain energy per unit area stored in the microstructures, is equal to

$$U_s = \frac{4}{d^2}U \tag{11}$$

i.e.,

$$U_s = \frac{2}{9}\frac{1}{d^2}(bhl)\frac{\sigma_{max}^2}{E} \tag{12}$$

Based on our configuration of the microstructures, and using $E = 8.3 \times 10^7$ kPa [9, 11], U_s at the yield point is approximately 12.1 $\mu J/cm^2$. This compares to 7.0 $\mu J/cm^2$ for oxidized silicon wafers joined by hydrophillic bonding. [3, 4]

This calculation assumes that the bond failure is associated with the simultaneous failure of all the microstructures. This is, of course, an idealization; a chain is only as strong as its weakest link. Nonuniform interlocking will result in a torque, as well as a tensile load, which would result in sequential, not simultaneous, microstructure yielding. This has the effect of lowering the apparent bond strength.

Piercing Microstructures

A primary application of this technology is to provide a means of joining or bonding to biologic tissues. Such a capability could be employed in several promising ways: vascular stents, wound or incision bandages, local drug delivery systems, and vascular anastomosis. The latter application represents an alternative to conventional suturing; instead of threading a polypropylene filament with a curved needle, a surgeon could join blood vessels using a connector whose surface is blanketed with the piercing microstructures.

Arrays of piercing microstructures (Figure 2), each approximately 4 μm $\times$ 4 μm, were fabricated and tested for gross adhesion capability. One-sided arrays, approximately 1 cm^2 square, were pressed into sections of a human vena cava obtained from a cadaver. The samples were successfully bonded to the tissue in this way, but the tensile strength is, as yet, below that required for clinical application. Electron micrographs of delaminated tissue show four distinct regions which are characterized by the following features:

1. Holes where the barbs have penetrated and retracted from the tissue.

2. Broken barbs where penetration and bonding have taken place, but the silicon pedestal supporting the pointed cap failed.

3. Intact pieces of silicon which remain bonded to the tissue. The silicon substrate itself fractured, probably during insertion.

4. Separation of the epithelial lining from the vessel wall, with the microstructure arrays remaining bonded to the lining.

This last situation is depicted in Figure 7, which shows the microstructures penetrating the epithelial membrane of the vena cava.

These results indicate the microstructures can be useful in bonding to biologic tissues, but the size and shape of the barbs must be optimized. In particular, it appears that the barbs are much smaller than needed for satisfactory latching, since the delamination is occuring within the vessel wall. We are currently exploring ways of building larger scale structures which will overcome this difficulty.

Summary

We have described two versions of a micromechanical fastening system based on silicon micromachining technology. Since the bonding mechanism in both types of structures is purely mechanical, it can be used in applications where chemical resistance, thermal tolerance, and/or biological compatibility are paramount. Successful demonstration of the bonding principle has been achieved for each version. Calculations of the tensile strength of the mating microstructures have been shown to be in approximate agreement with experimental results.

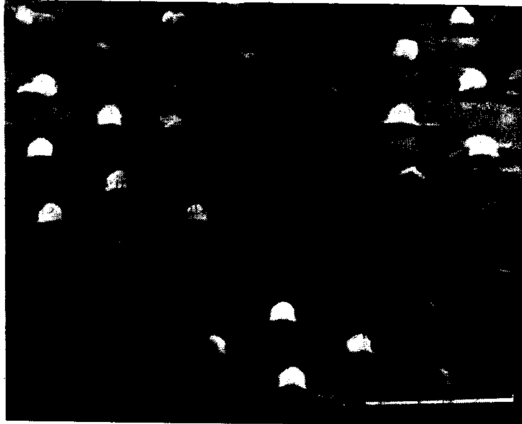

Figure 7: Piercing structures penetrating the epithelial membrane of a human vena cava. The remainder of the vessel wall has been excised to show the barbs.

Acknowledgements

The authors wish to thank M. Wholey, W. Novogradac, J. Suhan, C. Bowman, L. Rathbun, T. Schlesinger, W. Maly, and P. Steif for their assistance. This research was supported by the National Science Foundation, and has also benefited from an ongoing collaboration with Shadyside Hospital of Pittsburgh. Mask fabrication was performed at the National Nanofabrication Facility at Cornell University.

References

[1] X. Wu and W. H. Ko. Compensating corner undercutting in anisotropic etching of (100) silicon. *Sensors and Actuators* **18**, 207–215, 1989.

[2] J. Haisma, G. A. C. M. Spierings, U. K. P. Biermann, and J. A. Pals. Silicon-on-insulator wafer bonding-wafer thinning technological evaluations. *Jpn. J. Appl. Phys.* **28**(8), 1426–1443, 1989.

[3] V. Lehmann, U. Gosele, and K. Mitani. Contamination protection of semiconductor surfaces by wafer bonding. *Sol. St. Tech.* **33**(4), 91–92, 1990.

[4] W. P. Maszara, G. Goetz, A. Caviglia, and J. B. McKitterick. Bonding of silicon wafers for silicon-on-insulator. *J. Appl. Phys.* **64**(10), 4943–4950, 1988.

[5] J. B. Lasky. Wafer bonding for silicon-on-insulator technologies. *Appl. Phys. Lett.* **48**(1), 78–80, 1986.

[6] S. P. Timoshenko and J. M. Gere. *Mechanics of Materials.* D. Van Nostrand Company, 1972.

[7] E. P. Popov, S. Nagarajan, and Z. A. Lu. *Mechanics of Materials,* 2nd Edition. Prentice-Hall, 1976.

[8] S. P. Timoshenko. *Strength of Materials,* 3rd Edition. D. Van Nostrand Company, Inc, 1955.

[9] T. P. Weihs, S. Hong, J. C. Bravman, and W. D. Nix. Mechanical deflection of cantilever microbeams: a new technique for testing the mechanical properties of thin films. *J. Mater. Res.* **3**(5), 931–942, 1988.

[10] P. P. Gillis and J. J. Gilman. Double-cantilever mode of crack propagation. *J. Appl. Phys.* **35**(3), 647–658, 1964.

[11] K. E. Petersen and C. R. Guarnieri. Young's modulus measurements of thin films using micromechanics. *J. Appl. Phys.* **50**(11), 6761–6766, 1979.